Journal of Membrane Science 677 (2023) 121593

Contents lists available at ScienceDirect

Journal of Membrane Science

journal homepage: www.elsevier.com/locate/memsci

Enhancing the C3 separation performances of polycrystalline ZIF-8 membranes by additive-assisted secondary growth

Dong A. Kang [a], Hae-Kwon Jeong [a,b,*]

[a] Artie McFerrin Department of Chemical Engineering, Texas A&M University, 3122 TAMU, College Station, TX, 77843-3122, United States
[b] Department of Materials Science and Engineering, Texas A&M University, 3122 TAMU, College Station, TX, 77843-3122, United States

ARTICLE INFO

Keywords:
ZIF-8
Polycrystalline membranes
Propylene/propane separation
1,4-butanediol
Structural control

ABSTRACT

Polycrystalline zeolitic-imidazolate framework-8 (ZIF-8) membranes have shown very promising for propylene/propane (C3) separation. Though high-performance ZIF-8 membranes have been prepared by various synthesis methods, secondary growth method offers unique advantages due to its decoupling of a seeding step and a growth step, leading to membranes with better microstructures, thereby not only better separation performances but also higher reproducibility. However, there are only a few reports on ZIF-8 membranes with ultra-high C3 separation factors (i.e., >200) that are made by secondary growth method. Here, we report polycrystalline ZIF-8 membranes by a secondary growth method modified with an addition of 1,4-butanediol (Bdiol). The membranes showed significantly improved C3 separation factors up to ~283 as compared to those prepared without modification. It was found that adding Bdiol in the secondary growth solution improved the microstructures of the ZIF-8 membranes, thereby enhancing their C3 separation performances. Furthermore, the presence of Bdiol in the growth solution enabled formation of well-intergrown ZIF-8 membranes even with a low linker-to-metal ratio (~16), otherwise not possible to form ZIF-8 membranes. Interestingly, the resulting membranes showed a plate-like morphology with the highest separation factor of ~283 among those prepared. All membranes in this work exhibited enhanced C3 separation performances as compared to those synthesized without modification.

1. Introduction

ZIF-8, made of zinc ions tetrahedrally coordinated with 2-methylimidazolate (mIm), has attracted a great deal of research interest for propylene/propane (C3) separation due to its effective aperture size in the range of 4.0–4.2 Å which lies in between the molecular diameters of C3 molecules, thereby suitable for C3 separation based on the molecular sieving effect [1–4]. Ever since the report on the first ZIF-8 polycrystalline membranes exhibiting promising C3 separation in 2012 [5], there have been extensive works for the last decade or so to produce highly propylene-selective ZIF-8 membranes. Due to the polycrystalline nature of the membranes, however, it is of critical importance to improve the grain boundary structures (i.e., microscopic defects) of ZIF-8 membranes to achieve their high separation performances and reproducibility [6].

The grain boundary structures of polycrystalline ZIF-8 membranes, consequently their separation performances, are significantly affected by how they are processed. As such, various synthesis methods of ZIF-8 membranes have been developed and can be broadly classified into two categories: *in-situ* growth and secondary (seeded) growth [7,8]. In general, secondary growth method is considered better than *in-situ* growth in obtaining thinner membranes with better reproducibility due to the fact that nucleation and growth steps are decoupled in the secondary growth [6,9,10]. Furthermore, the decoupling of the nucleation and growth steps make it easier to control and improve the microstructures of ZIF-8 membranes by optimizing seeding and/or growth processes. For example, Lai and coworkers [5] reported the first ZIF-8 polycrystalline membranes for C3 separation by slip-coating ZIF-8 seed crystals and followed by secondary growth in an aqueous system. It was found that using water as a solvent in the secondary growth solution was a key to prepare well-intergrown ZIF-8 membranes with the C3 separation factor of ~35 [11]. Kwon et al. [12] reported a rapid microwave-assisted seeding technique, which enabled strong attachment and uniform distribution of seed crystals onto an α-alumina support, and subsequent secondary growth resulted in well-intergrown ZIF-8 membranes with the C3 separation factor of ~40. The same authors also prepared high-quality ZIF-8/ZIF-67 membranes through the heteroepitaxial growth of ZIF-67 from ZIF-8 seed layers seeded by the

* Corresponding author. Artie McFerrin Department of Chemical Engineering, Texas A&M University, 3122 TAMU, College Station, TX, 77843-3122, United States.
E-mail address: hjeong7@tamu.edu (H.-K. Jeong).

https://doi.org/10.1016/j.memsci.2023.121593
Received 3 February 2023; Received in revised form 14 March 2023; Accepted 17 March 2023
Available online 21 March 2023

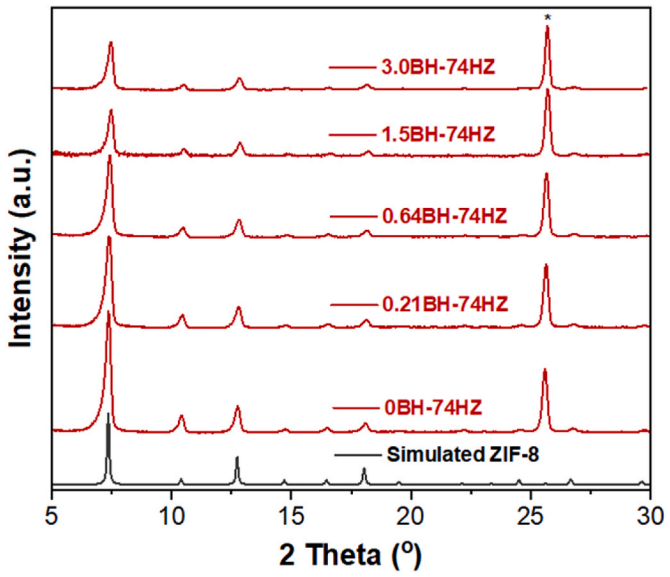

Fig. 1. XRD patterns of the membranes secondarily grown with the HmIm-to-Zn ratio (HZ) fixed at 74 with varying Bdiol-to-HmIm ratios (BH) (*: α-alumina support).

microwave-assisted seeding and the membranes showed impressively high C3 separation factor of ~209 [13]. The improved separation performance was attributed to enhanced grain boundary structure of heteroepitaxially grown ZIF layers and reduced effective aperture size of ZIF-67. Agrawal et al. [14] developed an electrophoretic nuclei assembly method where highly-packed ZIF-8 nuclei were deposited on a desired substrate driven by the electric field. The subsequent secondary growth of the seeded substrate resulted in the formation of a ZIF-8 membrane with the C3 separation factor of ~31.6. Recently, Kim et al. [15] showed that a silicalite seed layer on an anodic alumina oxide (AAO) substrate led to an increase in membrane-substrate bonding and enhancement in the C3 separation factor up to ~ 170. Lin et al. [16] reported that ZIF-8 seeding on a functionalized γ-alumina-coated α-alumina support enhanced bonding of a ZIF-8 seed layer with the support, minimizing intercrystalline defects and consequently leading to the high C3 separation factor of ~225.

On the other hand, there have been a few recent advancements in the *in-situ* growth of ZIF-8 membranes that showed impressive C3 separation performances. For example, Wang et al. [17] proposed an *in-situ* method based on a contra-diffusion concept where ZIF-8 membranes were synthesized on an amine-functionalized polymeric substrate. In the diffusion step, Zn ions could form covalent bonds with the amine groups on the substrate surface, consequently forming defect-free ZIF-8 membranes with the C3 separation factor of ~27.8. Very interestingly, Wang et al. [18] reported a current-driven synthesis technique which could produce ZIF-8 membranes exhibiting the impressive C3 separation factor of above 300 due to the electric-field-induced lattice distortion. Besides, there have been reported several promising unconventional approaches other than typical *in-situ* growth and secondary growth. For example, Li et al. [19] developed a gel-vapor deposition (GVD) method where a Zn-based gel layer coated on a polymeric hollow fiber was transformed to a well-intergrown ultra-thin ZIF-8 film via ligand vapor deposition, showing the C3 separation factor of ~70. Tsapatsis et al. [20] reported an all-vapor processing method where a ZnO layer was first deposited by atomic-layer deposition (ALD) onto a γ-alumina--coated α-alumina support, then transformed the ZnO layer into a ZIF-8-like structure by ligand-vapor treatment. The resulting membranes showed the C3 separation factor of ~70.

Despite its potential to achieve ZIF-8 membranes with better microstructure, however, secondary growth rarely led to ZIF-8 membranes with the C3 separation factors as high as ~300. It is our hypothesis that the separation performances of secondarily-grown ZIF-8 membranes can be further improved by optimizing the microstructures of ZIF-8 membranes via modification of secondary growth conditions.

As mentioned above, the grain boundary structures of ZIF-8 membranes determine their separation performances. As such, it is important to control the size and morphology of ZIF-8 crystals by adjusting synthesis conditions [21–27]. Wiebcke et al. [21] synthesized ZIF-8 nanocrystals by increasing the nucleation rate either via increasing the linker-to-metal ratio or introducing a basic modulator to promote the deprotonation of the linker. Gianneschi et al. [23] proposed mechanisms of ZIF-8 nucleation and growth using liquid cell transmission electron microscopy (LCTEM) analysis. According to their studies, ZIF-8 growth was limited by a surface process (i.e., movement of metal and ligand to edge sites and metal-ligand coordination), rather than the diffusion of monomer and ligand to a ZIF nucleus (i.e., transport process) while ZIF-8 nucleation is limited by local depletion of monomers (i.e., diffusion of monomers). More importantly, they confirmed that ZIF-8 size distribution was strongly affected by the nucleation rate, rather than the growth rate. Hong et al. [25] reported ZIF-8 with atypical morphologies such as flower-like and flake-like crystals by adding two additives: cetyltrimethylammonium bromide (CTAB) and tris(hydroxymethyl) aminomethane (TRIS). They found that additives preferentially adsorbed on a specific facet of ZIF-8 crystal, thereby decreasing its grow rate and consequently leading to the formation of atypical ZIF-8 morphologies.

Herein, we present how a simple addition of an additive, 1,4-butanediol, in the secondary growth solution significantly improves the microstructure of secondarily-grown ZIF-8 membranes, thereby enhancing their C3 separation performances. The effects of the additive in the secondary growth solution on the microstructures and morphologies of ZIF-8 membranes were systematically studied and thoroughly characterized. The C3 separation performances of the resulting membranes with different microstructures and morphologies were measured and compared with those reported in the literature.

2. Experimental

2.1. Materials

Zinc nitrate hexahydrate (ZnN, 98%), 2-methylimidazole (HmIm, 99%), sodium formate (SF, 99%), 1,4-butanediol (Bdiol, 99%), methanol (MeOH, >99.8%), methanol-d4 (CD_3OD-d_4, 99.8 atom% D), and sulfuric acid-d2 solution (D_2SO_4-d_2, 96–98 wt%) were purchased from Sigma Aldrich. All chemicals were used as received without further purifications.

2.2. Fabrication of ZIF-8 membranes using microwave-assisted seeding and secondary growth

Polycrystalline ZIF-8 membranes were fabricated using a rapid microwave-assisted seeding and subsequent secondary growth method on porous α-alumina disks (2.2 cm in diameter) as previously reported [12]. Alumina disks were prepared by following a procedure in our previous work [28]. For microwave-assisted seeding, a metal precursor solution (2.43 g of ZnN dissolved in 40 ml of MeOH) was prepared. An α-alumina disk, vertically fixed in a custom-made Teflon holder, was saturated by immersing and stirring it in the metal solution for 1 h using an orbital shaker. A ligand solution was prepared by dissolving 2.59 g of HmIm and 0.125 g of sodium formate (SF) in 30 ml of MeOH. The metal-solution-saturated disk was immersed in the ligand solution inside a microwave-inert glass tube, immediately followed by microwave radiation with the power of 100 W for 1.5 min in a microwave synthesizer (CEM, Discover-SP w/ActiVent®). After the reaction, the obtained seeded support was washed in MeOH under gentle shaking for 24 h and then dried in a convection oven at 60 °C for 4 h. For the secondary growth, a metal precursor solution (0.11 g of ZnN and x ml of Bdiol

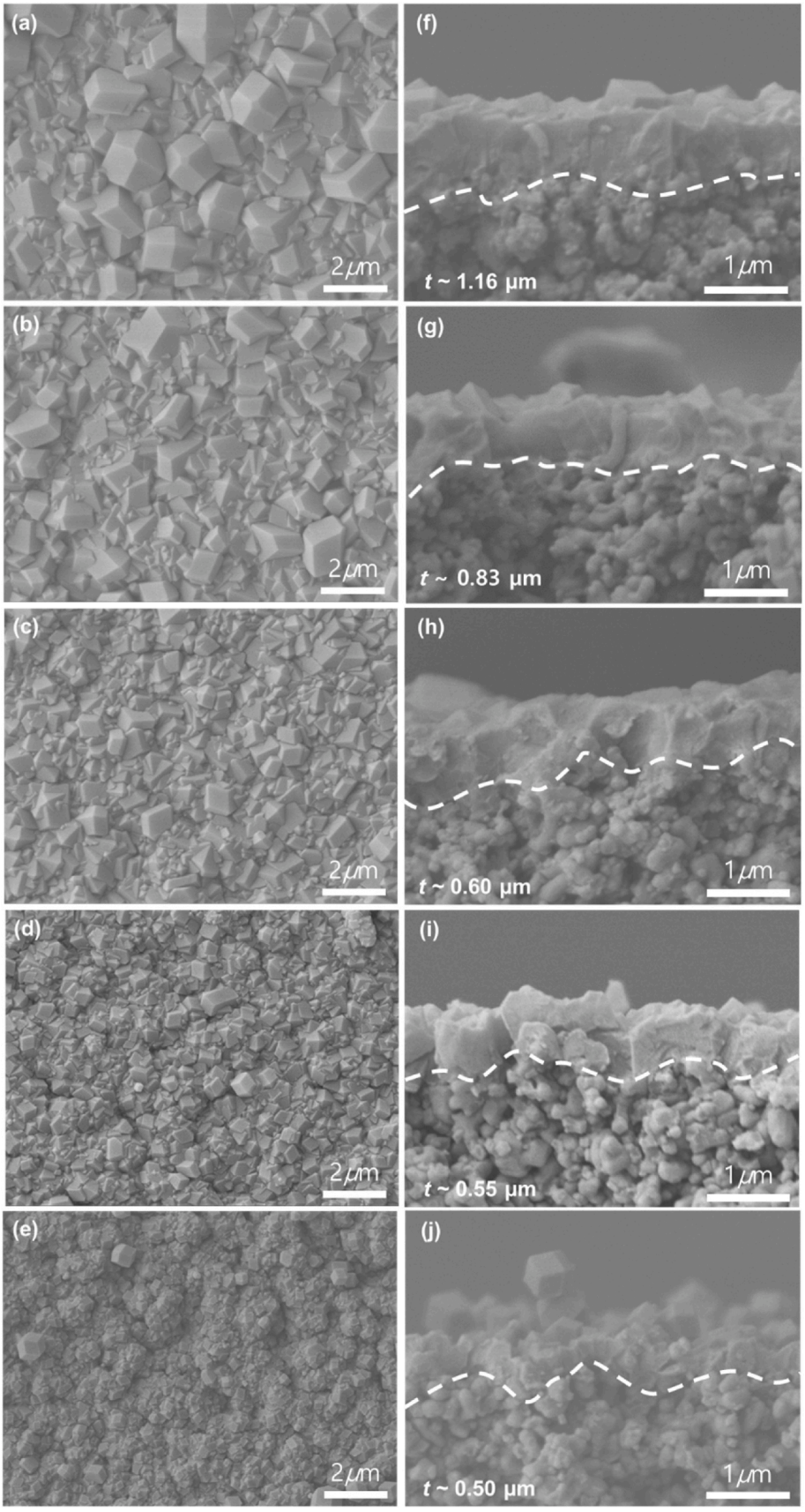

Fig. 2. SEM images of the membranes secondarily grown with the HmIm-to-Zn ratio (HZ) fixed at 74 with varying Bdiol-to-HmIm ratios (BH): (a, f) 0BH-74HZ, (b, g) 0.21BH-74HZ, (c, h) 0.64BH-74HZ, (d, i) 1.5BH-74HZ, and (e, j) 3.0BH-74HZ (*t*: thickness).

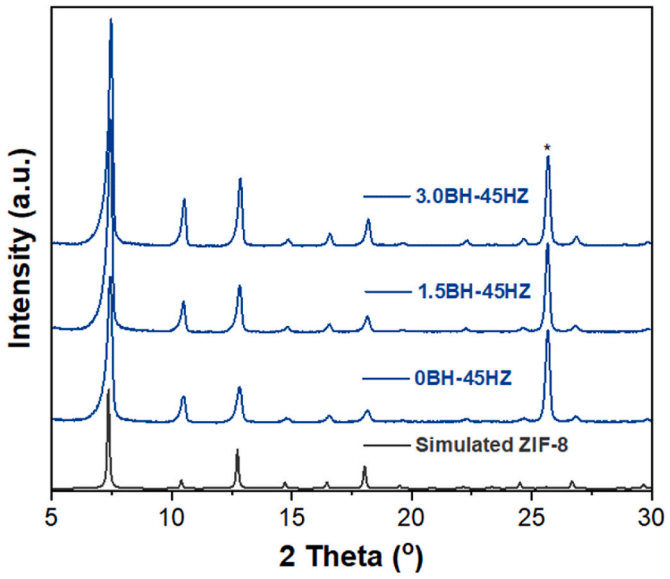

Fig. 3. XRD patterns of membranes prepared with the HmIm-to-Zn ratio (HZ) fixed at 45 with varying Bdiol-to-HmIm ratios (BH) (*: α-alumina support).

dissolved in 20 ml of DI water) and a ligand precursor solution (*y* g of HmIm in 20 ml of DI water) were prepared separately, where *x* and *y* were varied to adjust the molar ratios of Bdiol to HmIm (hereafter, BH) and HmIm to ZnN (hereafter, HZ) in the secondary growth solution. The resulting membranes were denoted as *a*BH-*b*HZ (*a* and *b* are the molar ratios) (see Fig. S1 and Table S1 for detailed combination of the molar ratios). For example, a 3.0BH-74HZ membrane was prepared in a secondary growth solution containing 3Bdiol: 1HmIm and 74HmIm: 1ZnN. The metal precursor solution was then poured into the ligand precursor solution and stirred using an orbital shaker for 1 min. The seeded disk placed vertically in the Teflon holder was immersed in the mixed precursor solution in a beaker. After covering with an aluminum foil, the beaker was placed in a convection oven at 30 °C for 16 h. The resulting membrane samples were washed in MeOH at room temperature for 2 d and then dried under a fume hood for 12 h.

2.3. Characterizations

X-ray diffraction (XRD) patterns were obtained using an X-ray diffractometer (Miniflex II, Rigaku) with Cu-Kα radiation (λ = 1.5406 Å). Scanning electron microscope (SEM) images were taken with a JEOL JSM-7500F operated at 5 keV of acceleration voltage using a lower secondary electron image (LEI) detector. N_2 physisorption isotherms were obtained using an ASAP 2020 plus (Micromeritics) at 77.3 K. Solution proton nuclear magnetic resonance (^{1}H NMR) measurements were conducted using Bruker Avance III. NMR samples were prepared by dissolving 14 mg of samples in 1.2 ml of CD_3OD-d_4 with 0.04 ml of D_2SO_4-d_2.

2.4. C3 gas permeation measurements

Equimolar C_3H_6/C_3H_8 binary gas separation properties of the ZIF-8 membranes were evaluated using the Wicke-Kallenbach technique at room temperature under the atmospheric pressure. The C3 gas mixture to a feed side and the argon sweeping gas to a permeate side were flowed at 100 cc/min, respectively. The composition of the permeate was analyzed by a gas chromatography (GC 7890A, Agilent) equipped with a flame ionized detector (FID) and a HP-plot Q column. The steady states of the membrane performances were declared after 12 h of measurements when changes in the GC peak areas of both propylene and propane were less than 5% over time. Permeation tests were conducted on three membranes produced under identical conditions to obtain the average and standard deviation of performances.

3. Results and discussions

3.1. Effects of Bdiol on the microstructure of ZIF-8 membranes

For control experiments, we first prepared ZIF-8 membranes with varying HmIm/Zn ratios in the secondary growth solution without Bdiol. It is noted that aqueous synthesis of ZIF-8 requires a relatively high ratio of HmIm to zinc nitrate more than 35 in the absence of modulating ligands [22,29]. This is because the excess HmIm is required to deprotonate the intermediate complex species, $[Zn(Hmim)_n]^{2+}$, for the formation of ZIF-8 crystal [22]. As expected, the XRD patterns (see Fig. S2) show that phase-pure ZIF-8 membranes were prepared only with relatively high HmIm to zinc ratios (i.e., 0BH-74HZ and 0BH-45HZ membranes). With a low HmIm to zinc ratio (i.e., 0BH-16HZ membrane), however, ZIF-L patterns were observed. At this low HmIm/Zn ratio, the intermediate $[Zn(Hmim)_n]^{2+}$ species are less likely deprotonated. As such, HmIm persists within the coordination compounds during the synthesis, consequently forming ZIF-L [30].

To see the effect of Bdiol in the secondary growth solution on the microstructure of ZIF-8 membranes, the ratio of Bdiol to HmIm (BH) was varied at a fixed HmIm/Zn ratio (HZ). Figs. 1–2 present the XRD patterns and SEM images of the membranes prepared at 74HZ in comparison with those of a ZIF-8 membrane prepared without Bdiol (0BH-74HZ).

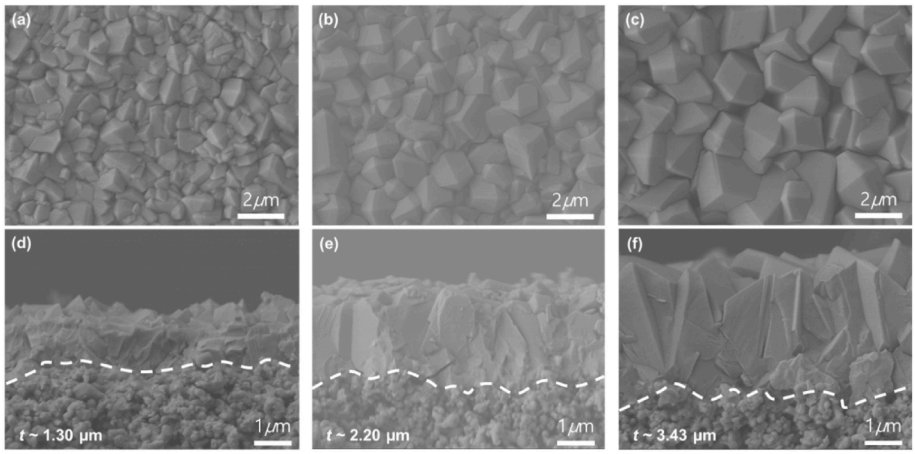

Fig. 4. SEM images of membranes prepared with the HmIm-to-Zn ratio (HZ) fixed at 45 with varying Bdiol-to-HmIm ratios (BH): (a, d) 0BH-45HZ, (b, e) 1.5BH-45HZ, and (c, f) 3.0BH-45HZ (*t*: thickness of ZIF-8 films).

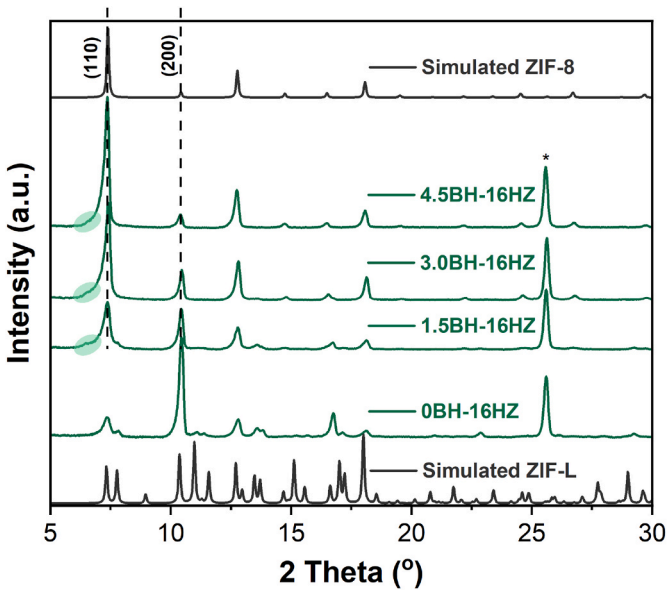

Fig. 5. XRD patterns of membranes prepared with the HmIm-to-Zn ratio (HZ) fixed at 16 with varying Bdiol-to-HmIm ratios (BH) (*: α-alumina support).

The XRD patterns in Fig. 1 show that regardless of the Bdiol/HmIm ratios, all samples are phase-pure ZIF-8 membranes. As the BH increases from 0 to 3, however, the diffraction peak intensities gradually decrease. As shown in the top SEM views (Fig. 2a–e), all membranes show the typical rhombic dodecahedron morphology of ZIF-8, but grain size becomes smaller as the additive concentration increases. At the BH less than 0.64, the membranes appear well intergrown (Fig. 2a–c). When the BH is further increased to 1.5 and above (Fig. 2d–e), the membranes are poorly intergrown, showing grain boundary defects. The cross-sectional views (Fig. 2f–j) reveal that the ZIF-8 membranes become thinner as the Bdiol concentration increases, which is consistent with the XRD results. These observations clearly show that Bdiol in the secondary growth solution modifies the growth conditions of ZIF-8 seed crystals, i.e., hinders their growth. This is because the basic nature of Bdiol (pK_a ~14.5) facilitates the deprotonation of HmIm in the growth solution, thereby promoting the homogenous nucleation of ZIF-8 (Scheme S1) [21,26,31]. Consequently, the growth of the ZIF-8 seed crystals is suppressed, thereby leading to a decrease in the grain size and the film thickness of the ZIF-8 membranes as the concentration of Bdiol increases at 74HZ. Figs. S4a–4b presents the SEM images of the ZIF-8 crystals obtained from the secondary growth solution (i.e., homogeneously nucleated crystals). As can be seen in the figure, the crystals from 1.5BH to 74HZ are smaller than those from 0BH to 74HZ in spite of a similar yield, suggesting that Bdiol promotes the homogenous nucleation of ZIF-8 as a deprotonator (i.e., the greater the homogeneous nucleation, the smaller the crystals become) [21,32].

We then investigated the effect of the HmIm-to-ZnN ratio (HZ ratio) by reducing the HZ ratio from 74 to 45. Figs. 3–4 show the XRD patterns and SEM images of the membranes synthesized with the fixed HZ ratio at 45 (i.e., 45HZ) and varying Bdiol-to-HmIm ratio (BH ratio). Fig. 3 presents the XRDs of the samples, showing all samples are phase-pure ZIF-8 membranes, regardless of the BH ratio at this HZ ratio of 45. The diffraction peak intensities increase as the Bdiol concentration increases, which is opposite of the case of 74HZ membranes. The SEM images (see Fig. 4a–c) shows that the grain size increases as the BH increases while the morphology of the grains maintains the typical rhombic dodecahedron of ZIF-8. Unlike the 0BH-45HZ and 1.5BH-45HZ membranes, the 3.0BH-45HZ membrane exhibits visibly noticeable grain boundary defects possibly due to its relatively bigger grains. A similar observation can be made in the cross-sectional views (Fig. 4d–f) wherein the membrane thickness increases as the additive concentration increases. The increased XRD intensities as the Bdiol concentration increases result from the increased ZIF-8 grain size and the thickness. Based on these observations, it is surmised that Bdiol acted as a promoting agent for the growth of ZIF-8 seed crystals under the current conditions. It is noted that the pK_a of Bdiol (~14.5) is higher than that of HmIm (~14.2), thereby facilitating the deprotonation of HmIm. The role of Bdiol in the growth of ZIF-8 seed crystals at 45HZ is opposite compared to that at 74HZ where Bdiol hinders the seed crystal growth as discussed in the previous paragraph. This is because the lower concentration of HmIm disfavors homogeneous nucleation at 45HZ than at 74HZ, thereby leading to the heterogeneous growth of seed crystals [21,23]. Indeed, the 0BH-45HZ growth solution led to formation of bigger crystals with lower yield than the 0BH-74HZ (Figs. S4a and S4c). Given the negligible change in crystal size observed at 45HZ (Figs. S4c and S4d) compared to at 74HZ (Figs. S4a and S4b), the addition of Bdiol to the secondary growth solution at 45HZ was less likely to promote the homogeneous nucleation of ZIF-8 due to the lower linker concentration [21–23]. At 45HZ, however, the growth of seed crystals is still promoted due to the deprotonated HmIm by Bdiol in the secondary growth solution. As a result, both grain size and membrane thickness increase as Bdiol concentration increases.

To further investigate the effect of the HZ, the HmIm-to-ZnN ratio was reduced to 16. Figs. 5–6 show the XRD patterns and SEM images of the resulting membranes synthesized with varying Bdiol concentration, respectively. As expected, no Bdiol in the secondary growth solution at 16HZ led to the formation of a ZIF-L membrane. With the Bdiol-to-HmIm ratio of 1.5 (i.e., 1.5BH) in the secondary growth solution, the membrane shows both ZIF-8 and ZIF-L patterns. Additionally, there is one unknown shoulder peak at 2θ ~6.5° as marked in Fig. 5, which also appears in all membranes synthesized with Bdiol in the secondary growth solution. As the BH ratio increased to 3.0 and 4.5, the obtained membranes show no ZIF-L peaks. As shown in the SEM images (Fig. 6b and f), the 1.5BH-16HZ membrane clearly exhibits a leaf-like morphology similar to the 0BH-16HZ membrane (ZIF-L membrane) (Fig. 6a and e). On the other hand, the 3.0BH-16HZ membrane shows a plate-like morphology with plates stacked along the in-plane direction (see Fig. 6c and g), noticeably different from the 1.5BH-16HZ membrane. Each plate is estimated approximately 80 nm in thickness (see the inset image in Fig. 6b). To confirm the phase change upon varying the BH ratio from 1.5 to 3.0, the N_2 adsorption isotherms on the membranes were taken (see Fig. S5) and the N_2 uptakes on the ZIF-8 layers were estimated by excluding those on the supports (see Fig. S6). As can be seen in Fig. S6, the 1.5BH-16HZ membrane appears similar to a ZIF-L membrane while the 3.0BH-16HZ membrane seems close to a ZIF-8 membrane (0BH-74HZ). Based on the XRD and N_2 isotherm analysis, therefore, it is confirmed that the 3.0BH-16HZ membrane is a ZIF-8 membrane exhibiting atypical morphology deviating from the typical dodecahedron of ZIF-8. It is known that ZIF-8 with atypical morphologies could be synthesized when additives such as modulating ligands or capping agents were used [25–27]. As such, it is our hypothesis that Bdiol acts as a capping agent competing with HmIm at the HZ ratio of 16, thereby resulting in different morphology. When the BH ratio is increased further from 3.0 to 4.5, however, a typical ZIF-8 morphology is observed (Fig. 6d). Based on these observations, it is speculated that the growth of ZIF-8 seed crystals is possible even at the low HmIm/Zn ratio of 16 when Bdiol is present in an aqueous growth solution due to the Bdiol-assisted deprotonation of HmIm. Since ZIF-L contains non-deprotonated HmIm in its structure [30], the low HmIm/Zn ratio of 16 in an aqueous solution results in low concentration of deprotonated HmIm, thereby leading to the formation of ZIF-L. In the presence of Bdiol, however, ZIF-8 can form even at the low HZ of 16 since Bdiol promotes the deprotonation of HmIm. When the Bdiol concentration is further increased (4.5BH-16HZ), a phase-pure ZIF-8 membrane with a typical ZIF-8 morphology is formed (Figs. 5, 6d and 6h). It is observed that the 3.0BH-16HZ and 4.5BH-16HZ show the noticeably different relative intensities of (200) and (110) peaks (see Fig. 5). The

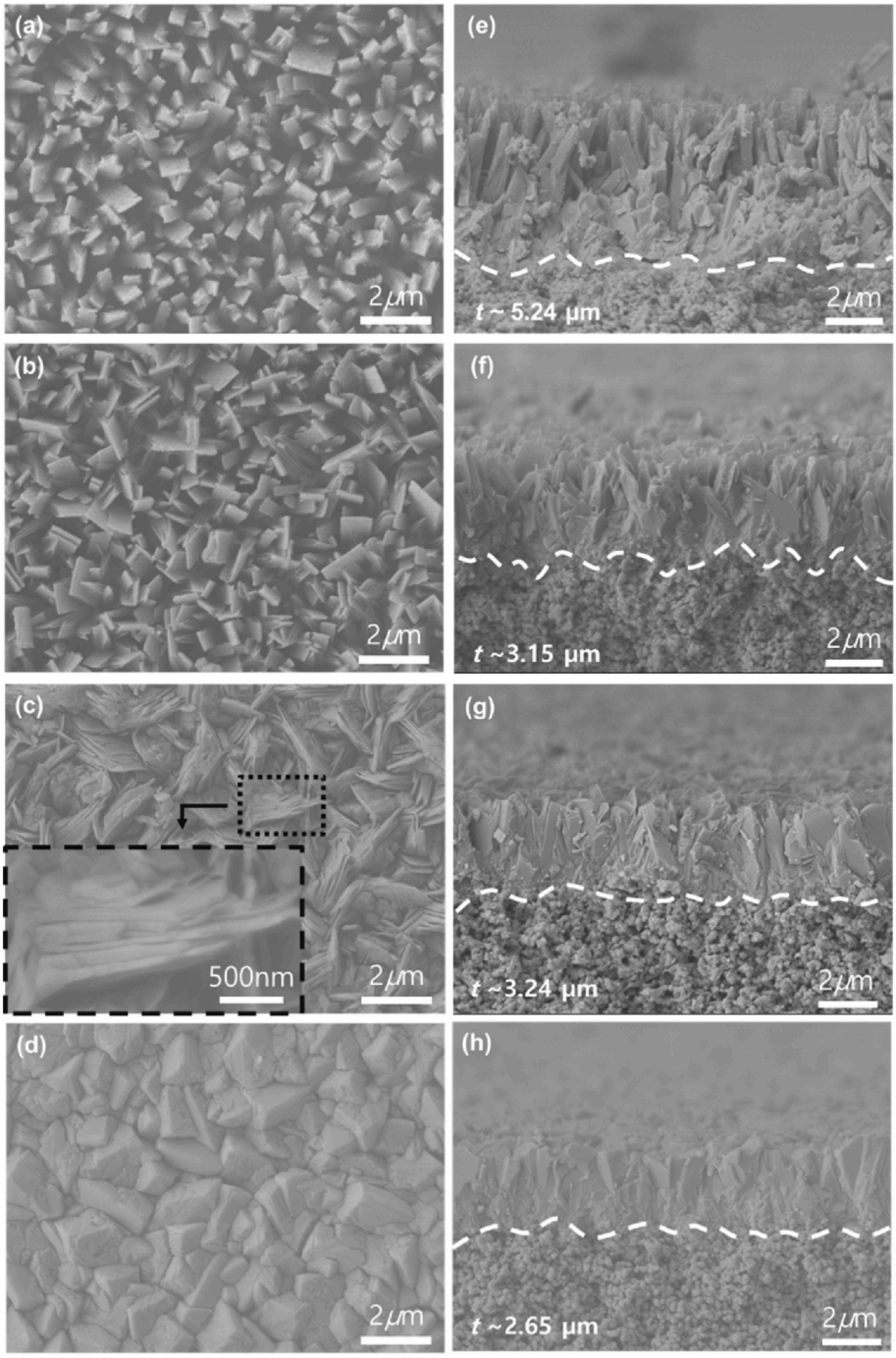

Fig. 6. SEM images of membranes prepared with the HmIm-to-Zn ratio (HZ) fixed at 16 with varying Bdiol-to-HmIm ratios (BH): (a, e) 0BH-16HZ, (b, f) 1.5BH-16HZ, (c, g) 3.0BH-16HZ, and (d, h) 4.5BH-16HZ (*t*: thickness).

3.0BH-16HZ membrane exhibits relatively strong preferred orientation along the [200] direction than the 4.5BH-16HZ membrane (see Table S3). It is hypothesized that at relatively low Bdiol concentrations (i.e., 3.0BH), Bdiol adsorbs mostly on the (110) plane than on the (200) plane, thus leading to the plate-like morphology with a preferred orientation along the <200> direction. At a relatively high BH ratio (i.e., 4.5), however, Bdiol may adsorb on both planes, consequently forming a typical ZIF-8 morphology with no preferred orientation. To check this hypothesis, ZIF-8 powders were collected from the growth solutions after membrane synthesis and the Bdiol-to-HmIm ratios incorporated into the framework were estimated using solution ^{1}H NMR (see Figs. S7a and S7b). As shown in Fig. S7b, the more Bdiol in the growth solution led to the more Bdiol incorporated in the ZIF-8 framework.

In summary, the observations thus far suggest that Bdiol acted as a deprotonator of HmIm in the growth solution (Scheme S1) [21,31] and its effect on the growth of seed crystals was, however, dependent on the linker-to-metal ratio (HZ). At the higher HZ of 74, as Bdiol concentration increased, concentration of deprotonated mIm anions in the grown solution increased, resulting in a relatively fast homogenous nucleation as compared to the heterogeneous nucleation, consequently thinner membranes with smaller grains (Figs. 1–2) [21,24]. In contrast, at the lower HZ of 45, the homogenous nucleation was suppressed due to the relatively low linker concentration, thereby promoting the

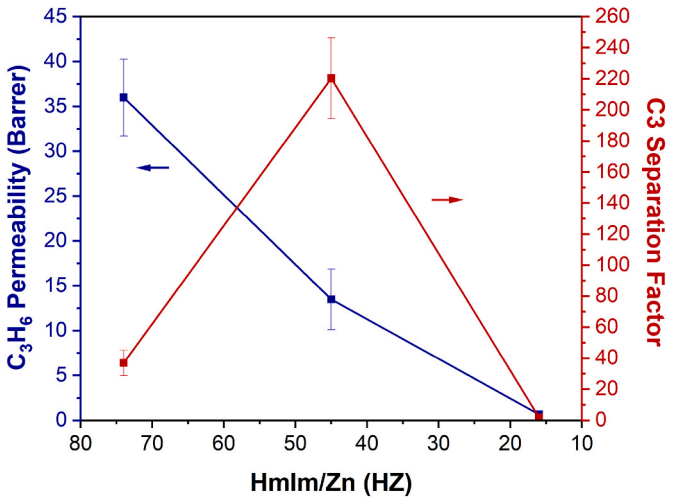

Fig. 7. C3 Separation performance of membranes synthesized without Bdiol.

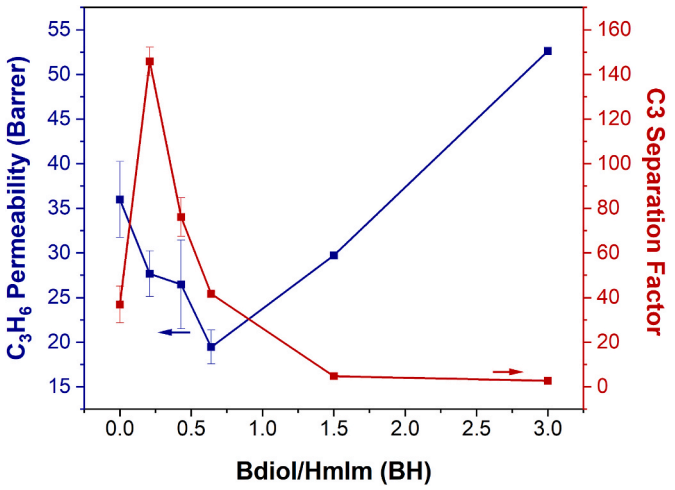

Fig. 8. C3 separation performances of ZIF-8 membranes synthesized with the HmIm-to-Zn ratio (HZ) fixed at 74 with varying Bdiol-to-HmIm ratios (BH).

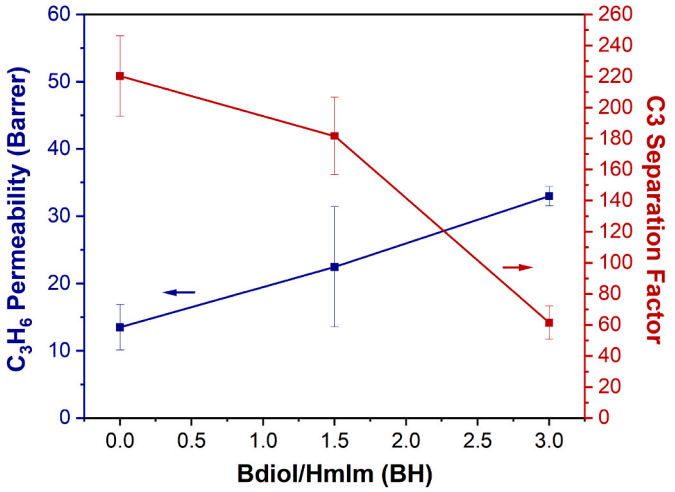

Fig. 9. C3 separation performances of ZIF-8 membranes synthesized with the HmIm-to-Zn ratio (HZ) fixed at 45 with varying Bdiol-to-HmIm ratios (BH).

heterogeneous growth of seed crystal and resulting in thicker

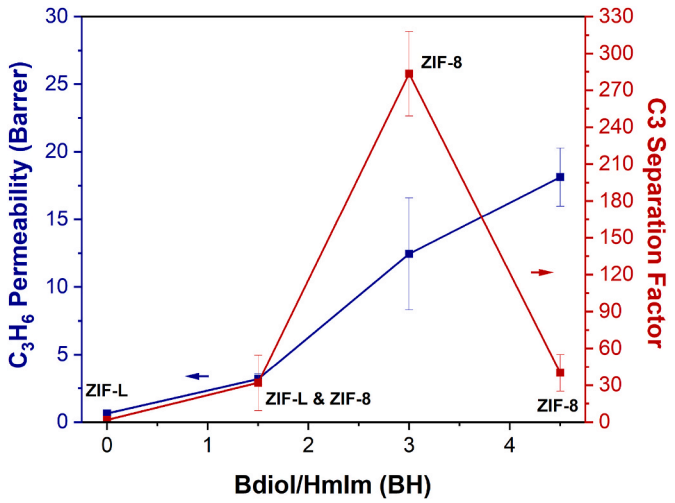

Fig. 10. C3 separation performances of ZIF-8 membranes synthesized with the HmIm-to-zinc ratio (HZ) fixed at 16 with varying Bdiol-to-HmIm ratios (BH).

membranes (Figs. 3–4) [21–23]. At the lowest HZ of 16, Bdiol enabled ZIF-8 formation by deprotonating the linker, while ZIF-L formed in the absence of Bdiol [22,26,30]. Furthermore, at the relatively high Bdiol concentration of 3.0BH-16HZ, the role of Bdiol as a capping agent became more apparent due to the low concentration of HmIm, leading to the atypical plate-like morphology possibly due to its preferential adsorption on the (110) planes (Figs. 5–6) [25,26,31].

3.2. C3 separation performances of membranes

Fig. 7 presents the C3 separation performances of the membranes prepared without Bdiol. The 0BH-74HZ membranes show a decent C3 separation performance with C3 separation factor of ~36.9 and C_3H_6 permeability of ~36.0 Barrer, comparable to those synthesized using secondary growth methods [5,12]. It is noted that the 0BH-74HZ membranes were prepared by growing ZIF-8 seeds in a typical aqueous secondary growth solution [5,11,12,15,33,34]. When the HmIm/Zn ratio decreased to 45, however, the membranes (i.e, 0BH-45HZ membranes) exhibit surprisingly high C3 separation factor of ~220 and C_3H_6 permeability of ~13.5 Barrer. As shown in Figs. S2–3, the 0BH-45HZ membrane exhibits smaller grains and lower XRD peak intensities than the 0BH-74HZ membrane. In general, the smaller the grains are, the better the grain boundary structure is, thereby showing better separation performances [12,35,36]. As such, the 0BH-45HZ membranes are likely to possess better grain boundaries, thereby showing increased separation factor and decreased permeability. When the HmIm/Zn ratio was further reduced to 16, however, ZIF-L membranes were formed, showing no C3 separation performance [30].

Fig. 8 and S8 present the separation performances of the membranes prepared at a HmIm-to-Zn ratio of 74 with varying Biol concentration. The performance can be divided into three regions: 1) 0–0.21BH, 2) 0.21–0.64BH and 3) 0.64 – 3BH. In the first region (0–0.21BH), as the BH increased, the C3 separation factor increased to ~ 145 while the C_3H_6 permeability decreased to ~ 27.7 Barrer. The 0.21BH-74HZ membranes show smaller grains than the 0BH-74HZ membranes (see Fig. 2a and b), thereby leading to better grain boundary structure and consequently enhanced C3 separation factor. In the second region (0.21–0.64BH), however, both C_3H_6 permeability and C3 separation factor decreased. It is hypothesized that the decreased separation performance might have to do with the incorporation of Bdiol in ZIF-8 frameworks. To investigate this, ZIF-8 powder samples were synthesized from the same secondary growth solutions for membranes. The powder samples were then characterized by solution ^{1}H NMR to investigate the Bdiol/HmIm ratios incorporated in the ZIF-8 frameworks.

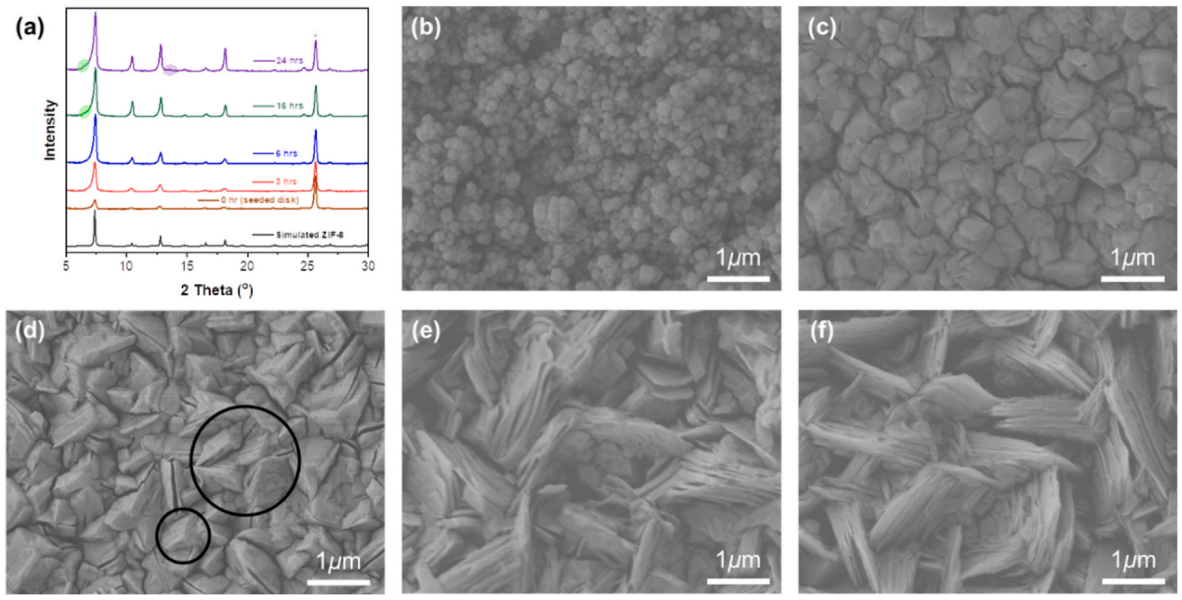

Fig. 11. The membranes prepared at the molar ratios of Bdiol to HmIm and HmIm to Zn fixed at 3.0 and 16, respectively, for different secondary growth time: (a) XRD patterns (*: α-alumina support) and top-view SEM images: (b) 0 h (seeded support), (c) 3 h, (d) 6 h, (e) 16 h, and (f) 24 h.

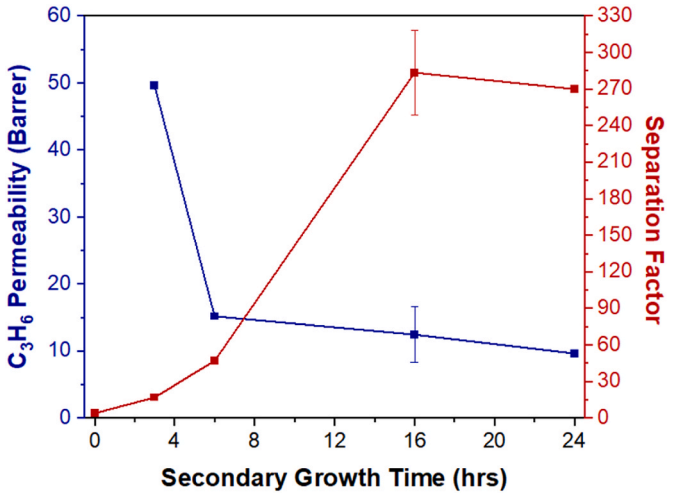

Fig. 12. C3 separation performances of ZIF-8 membranes synthesized at 3.0BH and 16HZ for varying secondary growth time.

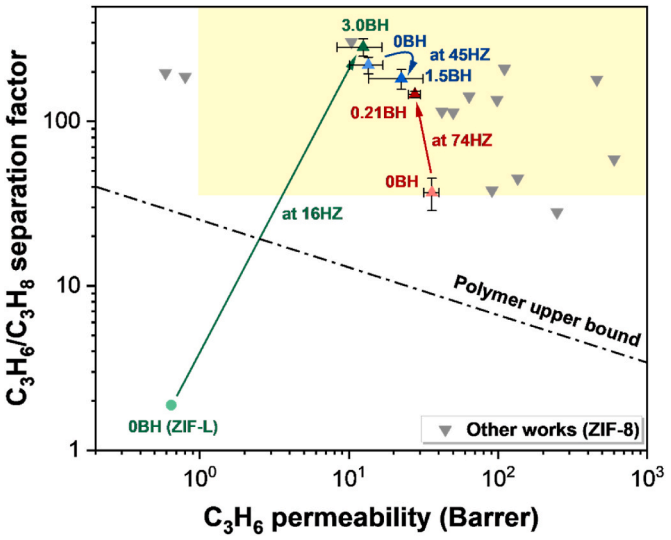

Fig. 13. C_3H_6/C_3H_8 separation performances of the ZIF-8 membranes in comparison with other membranes reported in the literature. The area marked in yellow is a so-called commercially attractive region [5,13,18,33,39–46]. (For interpretation of the references to colour in this figure legend, the reader is referred to the Web version of this article.)

Fig. S9a presents the ^{1}H NMR results and the Bdiol/HmIm ratio of the framework estimated from the NMR is plotted as a function of the Bdiol/HmIm ratio in the secondary growth solution (Fig. S9b). As more Bdiol is added in the secondary growth solution, more Bdiol was incorporated in the ZIF-8 powders. As can be seen in the figure, however, the Bdiol/HmIm ratio in the framework is three orders of magnitudes smaller than that in the growth solution. It is, therefore, likely that incorporation of the bulky Bdiol molecules is limited mostly to the ZIF-8 external surfaces via coordination with undersaturated zinc centers. Based on this observation, it is surmised that Bdiol coordinates with the undersaturated zinc centers of the surfaces of ZIF-8 grains (i.e., external and grain boundary surfaces) of the membranes, thereby reducing the grain boundary defects and consequently improving C3 separation performances (see the illustration presented in Fig. S10). If too many Bdiol molecules are incorporated, however, it could effectively block the selective intracrystalline pathways (i.e., 6-membered rings) of ZIF-8, leading to the decrease in both selectivity and permeability. In the third region (0.64BH – 3.0BH), the membranes showed little C3 separation performances with high C_3H_6 permeability. As shown in Fig. 2d and e, the 1.5BH-74HZ and 3.0BH-74HZ membranes exhibited poor grain boundary structure, resulting in poor separation performances as mentioned above.

Fig. 9 and S11 show the C3 separation performances of the membranes synthesized at a fixed HmIm-to-Zn ratio of 45 with varying Biol concentration. Unlike the 74HZ membranes, the 45HZ membranes showed increased permeability and decreased separation factor as the Bdiol concentration increased possibly due to poor grain boundaries with increasing size of grains as shown in Fig. 4a–c. In particular, there is a considerable drop in the separation factor going from 1.5BH (~181) to 3.0BH (~61.4) indicating the relatively poor grain boundary structure of the 3.0BH-45HZ membrane (see Fig. 4c). Compared to the 0BH-45HZ membrane, the 1.5BH-45HZ membrane showed 69.5% increase in C_3H_6

permeability (~22.4 Barrer) and 17.5% decrease in C3 separation factor (~181.7).

Fig. 10 and S12 present the C3 separation performances of the membranes prepared at a fixed HmIm-to-Zn ratio of 16 with varying Biol concentration. As discussed above, the 0BH-16HZ membranes (ZIF-L membranes) show no C3 separation performance. The 1.5BH-16HZ membranes show the C3 separation factor of ~32.0 with the low C_3H_6 permeability of ~3 Barrer. It is reminded that the 1.5BH-16HZ membrane contains ZIF-L as a major phase. Because of the presence of the non-permeable ZIF-L, the membrane shows low C_3H_6 permeability. With 3.0BH, the membranes (3.0BH-16HZ) show surprisingly high C3 separation factor of ~283, the highest among those prepared in this work, while with 4.5BH, the C3 separation factor dropped to ~ 40.1. It is noted that the 3.0BH-16HZ membranes show plate-like morphology, somewhat similar but different from the leaf-like morphology of ZIF-L. It is our hypothesis that the unexpectedly high C3 separation performance of the 3.0BH-16HZ membranes might have to do with this unique ZIF-8 morphology. As shown in Fig. 5 and discussed above, the 3.0BH-16HZ membranes exhibit relatively strong preferred orientation along the [200] direction as compared to the 4.5BH-16HZ membrane (see Table S3) [37,38]. It is noted that the 1.5BH-16HZ membrane was excluded since the membrane showed distinct ZIF-L diffraction peaks overlapping with ZIF-8 peaks (e.g., (020) of ZIF-L overlaps with (200) of ZIF-8). The (200)-oriented 3.0BH-16HZ membranes, likely due to the plate-like morphology, possess much improved grain boundary structure, thereby significantly enhanced C3 separation capability.

Given the interesting morphology and outstanding C3 separation performance exhibited by the 3.0BH-16HZ membranes with a secondary growth time of 16 h, the evolution of both morphology and performance was further investigated as a function of the growth time. Fig. 11 presents the XRD patterns and SEM images of the resulting membranes (see Fig. S13 for cross-sectional views). As growth time increases, the diffraction intensities of the membranes were increased due to the increased thickness of the membranes. When the growth time was 3 h, the membrane showed phase-pure ZIF-8 pattern (Fig. 11a) and poorly defined polyhedron grain morphology (Fig. 11c). At 6 h of growth time, however, plate-like morphologies were locally observed as marked (Fig. 11d). With the growth time longer than 16 h, plate-like morphology was observed (Fig. 11e and f) and the unknown shoulder peak appeared at 2θ ~6.5° as previously discussed (Fig. 11a). For 24 h of growth time, another unknown peak at 2θ ~13.7° was observed with more plate-like morphology. Fig. S14 presents the crystallographic preferred orientation (CPO) of (200)/(110) of the membranes as secondary growth time increases. The membranes with plate-like morphology exhibit much higher CPO values (i.e., preferred out-of-plane orientation along the [200] direction). Fig. 12 and S15 shows the C3 separation performance of the 3.0BH-16HZ membranes prepared for different secondary growth time. Up to 6 h of growth, the membranes showed gradual increase and decrease in C3 separation factor and permeability, respectively. This can be attributed to improved grain boundary structure of the membranes. However, at 16 h of growth time when the membrane shows plate-like morphology, the membrane exhibited a drastic increase in C3 separation factor while there is little change in C3 permeability. Additional growth for 24 h resulted in no further change in both permeability and separation factor.

Fig. 13 and Table S4 compare the C3 separation performances of the membranes in this work with other high-performance polycrystalline ZIF-8 membranes reported in the literature. To the best of our knowledge, the 3.0BH-16HZ membranes with the C3 separation factor of ~283 are among the most C3-selective ZIF-8 membranes, outperforming most of the previously reported membranes.

4. Conclusion

In conclusion, we investigated the effects of Bdiol as an additive on the structure and microstructure of ZIF-8 membranes by the secondary growth method. With Bdiol, high-quality ZIF-8 membranes were synthesized even at the low HmIm/Zn ratio of 16, while ZIF-L membranes were formed at this HmIm/Zn ratio without the additive. This is attributed to the basic nature of Bdiol facilitating the deprotonation of HmIm. It was found that the effects of Bdiol depended upon the HmIm/Zn ratios of the secondary growth solutions: at relatively high HmIm concentration (i.e., 74HZ), Bdiol promotes homogenous ZIF-8 nucleation, thereby suppressing the growth of ZIF-8 seed crystals. On the other hand, at lower HZ conditions (45HZ and 16HZ), Bdiol facilitates the growth of seed crystals since homogeneous nucleation is restrained due to the lower concentration of HmIm. At 16HZ, Bdiol acts as a capping agent as well, forming the atypical ZIF-8 morphology. The 3.0BH-16HZ membrane exhibited the plate-like morphology and showed ultra-high C3 separation factor of ~283, which is one of the highest among those reported so far. It was hypothesized that the unique morphology and unexpectedly high C3 separation performance of the 3.0BH-16HZ membranes might be due to the preferentially-oriented growth of ZIF-8 along the [200] direction, leading to significantly improved grain boundary structure and consequently enhancing C3 separation performance.

Authors statement

Donga Kang: Conceptualization, Methodology, Writing- Original draft preparation, Investigation. Hae-Kwon Jeong:Supervision, Writing-Reviewing and Editing.

Declaration of competing interest

The authors declare that they have no known competing financial interests or personal relationships that could have appeared to influence the work reported in this paper.

Data availability

Data will be made available on request.

Acknowledgements

H.-K.J. acknowledges the financial support from the National Science Foundation (CBET-1929596). This publication was made possible in part by NPRP grant # 12S-0209-190064 from the Qatar National Research Fund (a member of Qatar Foundation). The findings achieved herein are solely the responsibility of the authors. The National Science Foundation supported the FE-SEM acquisition under Grant DBI-0116835, the VP for Research Office, and the Texas A&M Engineering Experimental Station.

Appendix A. Supplementary data

Supplementary data to this article can be found online at https://doi.org/10.1016/j.memsci.2023.121593.

References

[1] K.S. Park, Z. Ni, A.P. Côté, J.Y. Choi, R. Huang, F.J. Uribe-Romo, H.K. Chae, M. O'Keeffe, O.M. Yaghi, Exceptional chemical and thermal stability of zeolitic imidazolate frameworks, Proc. Natl. Acad. Sci. USA 103 (27) (2006) 10186–10191.
[2] C. Zhang, R.P. Lively, K. Zhang, J.R. Johnson, O. Karvan, W.J. Koros, Unexpected molecular sieving properties of zeolitic imidazolate framework-8, J. Phys. Chem. Lett. 3 (16) (2012) 2130–2134.
[3] H.T. Kwon, H.-K. Jeong, In situ synthesis of thin zeolitic–imidazolate framework ZIF-8 membranes exhibiting exceptionally high propylene/propane separation, J. Am. Chem. Soc. 135 (29) (2013) 10763–10768.
[4] J. Yao, H. Wang, Zeolitic imidazolate framework composite membranes and thin films: synthesis and applications, Chem. Soc. Rev. 43 (13) (2014) 4470–4493.
[5] Y. Pan, T. Li, G. Lestari, Z. Lai, Effective separation of propylene/propane binary mixtures by ZIF-8 membranes, J. Membr. Sci. 390 (2012) 93–98.

[6] Y. Ren, X. Liang, H. Dou, C. Ye, Z. Guo, J. Wang, Y. Pan, H. Wu, M.D. Guiver, Z. Jiang, Membrane-based olefin/paraffin separations, Adv. Sci. 7 (19) (2020), 2001398.
[7] B. Freeman, Y. Yampolskii, I. Pinnau, Materials Science of Membranes for Gas and Vapor Separation, John Wiley & Sons, 2006.
[8] M. Shah, M.C. McCarthy, S. Sachdeva, A.K. Lee, H.-K. Jeong, Current status of metal–organic framework membranes for gas separations: promises and challenges, Ind. Eng. Chem. Res. 51 (5) (2012) 2179–2199.
[9] N. Rangnekar, N. Mittal, B. Elyassi, J. Caro, M. Tsapatsis, Zeolite membranes–a review and comparison with MOFs, Chem. Soc. Rev. 44 (20) (2015) 7128–7154.
[10] Z.Y. Yeo, S.-P. Chai, P.W. Zhu, A.R. Mohamed, An overview: synthesis of thin films/membranes of metal organic frameworks and its gas separation performances, RSC Adv. 4 (97) (2014) 54322–54334.
[11] Y. Pan, Z. Lai, Sharp separation of C2/C3 hydrocarbon mixtures by zeolitic imidazolate framework-8 (ZIF-8) membranes synthesized in aqueous solutions, Chem. Commun. 47 (37) (2011) 10275–10277.
[12] H.T. Kwon, H.-K. Jeong, Highly propylene-selective supported zeolite-imidazolate framework (ZIF-8) membranes synthesized by rapid microwave-assisted seeding and secondary growth, Chem. Commun. 49 (37) (2013) 3854–3856.
[13] H.T. Kwon, H.-K. Jeong, A.S. Lee, H.S. An, J.S. Lee, Heteroepitaxially grown zeolitic imidazolate framework membranes with unprecedented propylene/propane separation performances, J. Am. Chem. Soc. 137 (38) (2015) 12304–12311.
[14] G. He, M. Dakhchoune, J. Zhao, S. Huang, K.V. Agrawal, Electrophoretic nuclei assembly for crystallization of high-performance membranes on unmodified supports, Adv. Funct. Mater. 28 (20) (2018), 1707427.
[15] S. Dangwal, A. Ronte, H. Lin, R. Liu, J. Zhu, J.S. Lee, H. Gappa-Fahlenkamp, S.-J. Kim, ZIF-8 membranes supported on silicalite-seeded substrates for propylene/propane separation, J. Membr. Sci. 626 (2021), 119165.
[16] F. Banihashemi, J.Y. Lin, Synthesis of ZIF-8 membranes on γ-alumina supports for separation of propylene/propane gas mixture, Ind. Eng. Chem. Res. 61 (11) (2022) 4125–4133.
[17] E. Shamsaei, X. Lin, Z.-X. Low, Z. Abbasi, Y. Hu, J.Z. Liu, H. Wang, Aqueous phase synthesis of ZIF-8 membrane with controllable location on an asymmetrically porous polymer substrate, ACS Appl. Mater. Interfaces 8 (9) (2016) 6236–6244.
[18] S. Zhou, Y. Wei, L. Li, Y. Duan, Q. Hou, L. Zhang, L.-X. Ding, J. Xue, H. Wang, J. Caro, Paralyzed membrane: current-driven synthesis of a metal-organic framework with sharpened propene/propane separation, Sci. Adv. 4 (10) (2018), eaau1393.
[19] W. Li, P. Su, Z. Li, Z. Xu, F. Wang, H. Ou, J. Zhang, G. Zhang, E. Zeng, Ultrathin metal–organic framework membrane production by gel–vapour deposition, Nat. Commun. 8 (1) (2017) 1–8.
[20] X. Ma, P. Kumar, N. Mittal, A. Khlyustova, P. Daoutidis, K.A. Mkhoyan, M. Tsapatsis, Zeolitic imidazolate framework membranes made by ligand-induced permselectivation, Science 361 (6406) (2018) 1008–1011.
[21] J. Cravillon, R. Nayuk, S. Springer, A. Feldhoff, K. Huber, M. Wiebcke, Controlling zeolitic imidazolate framework nano-and microcrystal formation: insight into crystal growth by time-resolved in situ static light scattering, Chem. Mater. 23 (8) (2011) 2130–2141.
[22] M. Jian, B. Liu, R. Liu, J. Qu, H. Wang, X. Zhang, Water-based synthesis of zeolitic imidazolate framework-8 with high morphology level at room temperature, RSC Adv. 5 (60) (2015) 48433–48441.
[23] J.P. Patterson, P. Abellan, M.S. Denny Jr., C. Park, N.D. Browning, S.M. Cohen, J. E. Evans, N.C. Gianneschi, Observing the growth of metal–organic frameworks by in situ liquid cell transmission electron microscopy, J. Am. Chem. Soc. 137 (23) (2015) 7322–7328.
[24] C.-W. Tsai, E.H. Langner, The effect of synthesis temperature on the particle size of nano-ZIF-8, Microporous Mesoporous Mater. 221 (2016) 8–13.
[25] G. Zheng, Z. Chen, K. Sentosun, I. Pérez-Juste, S. Bals, L.M. Liz-Marzán, I. Pastoriza-Santos, J. Pérez-Juste, M. Hong, Shape control in ZIF-8 nanocrystals and metal nanoparticles@ ZIF-8 heterostructures, Nanoscale 9 (43) (2017) 16645–16651.
[26] I.U. Khan, M.H.D. Othman, A. Ismail, N. Ismail, J. Jaafar, H. Hashim, M. A. Rahman, A. Jilani, Structural transition from two-dimensional ZIF-L to three-dimensional ZIF-8 nanoparticles in aqueous room temperature synthesis with improved CO2 adsorption, Mater. Char. 136 (2018) 407–416.
[27] L. Hu, Z. Yan, X. Mo, X. Peng, L. Chen, Morphology control synthesis of ZIF-8 as highly efficient catalyst for the cycloaddition of CO2 to cyclic carbonate, ChemCatChem 11 (14) (2019) 3212–3219.
[28] M.J. Lee, H.T. Kwon, H.K. Jeong, High-flux zeolitic imidazolate framework membranes for propylene/propane separation by postsynthetic linker exchange, Angew. Chem. Int. Ed. 57 (1) (2018) 156–161.
[29] Y. Pan, Y. Liu, G. Zeng, L. Zhao, Z. Lai, Rapid synthesis of zeolitic imidazolate framework-8 (ZIF-8) nanocrystals in an aqueous system, Chem. Commun. 47 (7) (2011) 2071–2073.
[30] R. Chen, J. Yao, Q. Gu, S. Smeets, C. Baerlocher, H. Gu, D. Zhu, W. Morris, O. M. Yaghi, H. Wang, A two-dimensional zeolitic imidazolate framework with a cushion-shaped cavity for CO 2 adsorption, Chem. Commun. 49 (82) (2013) 9500–9502.
[31] M. He, J. Yao, Q. Liu, K. Wang, F. Chen, H. Wang, Facile synthesis of zeolitic imidazolate framework-8 from a concentrated aqueous solution, Microporous Mesoporous Mater. 184 (2014) 55–60.
[32] Z. Öztürk, M. Filez, B.M. Weckhuysen, Decoding nucleation and growth of zeolitic imidazolate framework thin films with atomic force microscopy and vibrational spectroscopy, Chem.–Eur. J. 23 (45) (2017) 10915–10924.
[33] N.T. Tran, J. Kim, M.R. Othman, Microporous ZIF-8 membrane prepared from secondary growth for improved propylene permeance and selectivity, Microporous Mesoporous Mater. 285 (2019) 178–184.
[34] D. Liu, X. Ma, H. Xi, Y. Lin, Gas transport properties and propylene/propane separation characteristics of ZIF-8 membranes, J. Membr. Sci. 451 (2014) 85–93.
[35] S. Tanaka, K. Okubo, K. Kida, M. Sugita, T. Takewaki, Grain size control of ZIF-8 membranes by seeding-free aqueous synthesis and their performances in propylene/propane separation, J. Membr. Sci. 544 (2017) 306–311.
[36] C. Chen, A. Ozcan, A.O. Yazaydin, B.P. Ladewig, Gas permeation through single-crystal ZIF-8 membranes, J. Membr. Sci. 575 (2019) 209–216.
[37] A.D. French, Idealized powder diffraction patterns for cellulose polymorphs, Cellulose 21 (2) (2014) 885–896.
[38] C. Chang, C. Lee, J. Huang, Relationship between grain size and Zener–Holloman parameter during friction stir processing in AZ31 Mg alloys, Scripta Mater. 51 (6) (2004) 509–514.
[39] C.W. Colling, G.A. Huff Jr., J.V. Bartels, Processes Using Solid Perm-Selective Membranes in Multiple Groups for Simultaneous Recovery of Specified Products from a Fluid Mixture, 2004. US.
[40] N. Hara, M. Yoshimune, H. Negishi, K. Haraya, S. Hara, T. Yamaguchi, Thickness reduction of the zeolitic imidazolate framework-8 membrane by controlling the reaction rate during the membrane preparation, J. Chem. Eng. Jpn. 47 (10) (2014) 770–776.
[41] N. Hara, M. Yoshimune, H. Negishi, K. Haraya, S. Hara, T. Yamaguchi, Diffusive separation of propylene/propane with ZIF-8 membranes, J. Membr. Sci. 450 (2014) 215–223.
[42] H.T. Kwon, H.-K. Jeong, Improving propylene/propane separation performance of Zeolitic-Imidazolate framework ZIF-8 Membranes, Chem. Eng. Sci. 124 (2015) 20–26.
[43] K. Eum, C. Ma, A. Rownaghi, C.W. Jones, S. Nair, ZIF-8 membranes via interfacial microfluidic processing in polymeric hollow fibers: efficient propylene separation at elevated pressures, ACS Appl. Mater. Interfaces 8 (38) (2016) 25337–25342.
[44] Z. Lai, Development of ZIF-8 membranes: opportunities and challenges for commercial applications, Current opinion in chemical engineering 20 (2018) 78–85.
[45] W. Li, W. Wu, Z. Li, J. Shi, Y. Xia, Sol–gel asynchronous crystallization of ultra-selective metal–organic framework membranes for gas separation, J. Mater. Chem. 6 (34) (2018) 16333–16340.
[46] R. Wei, H.Y. Chi, X. Li, D. Lu, Y. Wan, C.W. Yang, Z. Lai, Aqueously cathodic deposition of ZIF-8 membranes for superior propylene/propane separation, Adv. Funct. Mater. 30 (7) (2020), 1907089.